Ethylene-bridged Mesoporous Organosilicas with Hexagonal and Cubic Symmetry

Yucang Liang[a,b], Egil Sev. Erichsen[c], Marianne Hanzlik[d], and Reiner Anwander[a,b]

[a] Institut für Anorganische Chemie, Universität Tübingen, Auf der Morgenstelle 18, D-72076 Tübingen, Germany
[b] Department of Chemistry, University of Bergen, Allégaten 41, N-5007, Bergen, Norway
[c] Laboratory for Electron Microscopy, University of Bergen, Allégaten 41, N-5007, Bergen, Norway
[d] Institut für Technische Chemie, Technische Universität München, Lichtenbergstraße 4, D-85747 Garching, Germany

Reprint requests to Prof. Dr. Reiner Anwander. Fax: +49(0)7071/29 2436.
E-mail: reiner.anwander@uni-tuebingen.de

Z. Naturforsch. **2009**, *64b,* 1289 – 1304; received September 28, 2009

Dedicated to Professor Hubert Schmidbaur on the occasion of his 75th birthday

A series of ordered periodic mesoporous organosilicas (PMOs) with cubic and hexagonal symmetries were fabricated by using divalent surfactants $[CH_3(CH_2)_{15}NMe_2(CH_2)_3NMe_3]^{2+}$ $2Br^-$ ($C_{16\text{-}3\text{-}1}$) or binary surfactant mixtures $[CH_3(CH_2)_{15}NMe_3]^+$ Br^- (C_{16}TABr) and $C_{16\text{-}3\text{-}1}$ as structure-directing agents (SDAs) and 1,2-bis(triethoxysilyl)ethane (BTEE) as an organosilica source under various basic conditions. The shape/structure of surfactant, molar ratio of binary surfactant mixtures, and base concentration crucially affect the formation of distinct mesophases. Face-centered cubic $Fm\bar{3}m$ mesoporous organosilicas can be obtained by using various concentrations of divalent surfactant $C_{16\text{-}3\text{-}1}$ or equimolar mixtures of divalent and monocationic surfactants as SDAs under basic conditions. Cubic $Pm\bar{3}n$ or 2D hexagonal *p6mm* mesophases can be synthesized by changing the molar ratio of the binary surfactant mixtures or the amount of the base NaOH. Use of monocationic C_{16}TABr instead of $C_{16\text{-}3\text{-}1}$ as template produced the hexagonal *p6mm* mesophase exclusively independent of the amount of the surfactant and the base. In addition, use of trimethylbenzene as expander molecule in the aforementioned binary surfactant template system caused a mesophase transformation from cubic $Pm\bar{3}n$ to *p6mm* symmetry. All samples were characterized by powder X-ray diffraction (PXRD) analysis and N_2 physisorption. The formation of face-centered cubic $Fm\bar{3}m$, primary cubic $Pm\bar{3}n$, and hexagonal *p6mm* PMOs was also confirmed by transmission electron microscopy (TEM), revealing a good long-range ordering with regular arrays. Moreover, variation of the synthesis parameters resulted in a variety of different PMO morphologies, as ascertained by scanning electron microscopy (SEM). FT-IR and solid-state ^{13}C and ^{29}Si NMR spectroscopy further revealed that the organic groups were uniformly incorporated into the framework. The various BET surface areas of the PMOs range from 470 to 780 $m^2\,g^{-1}$, while the pore diameters lie within a 26 to 30 Å range, as derived from N_2 physisorption.

Key words: Organosilicas, Cationic Surfactants, Mesoporous, Mesophase Transformation, Morphology

Introduction

Periodic mesoporous organosilicas (PMOs), featuring (metal)organic groups covalently incorporated into the inorganic framework [1 – 4], have attracted considerable attention for applications in optics, separation, and catalysis due to uniform distribution of the (metal)organic functionalities [5 – 15]. Cationic [1 – 4, 6 – 11, 16 – 27], anionic [28, 29], as well as neutral surfactants [30], and various commercially available block copolymers [6, 8, 9, 12, 13, 27, 31 – 42] have been used as structure-directing agents (SDAs) under basic or acidic conditions to fabricate mesoporous organosilicas with 2D hexagonal *p6mm* [1 – 4, 17 – 26, 31 – 36, 39, 40], 3D hexagonal $P6_3/mmc$ [1, 20], 3D cubic $Pm\bar{3}n$ [16, 21, 23, 28, 29], $Im\bar{3}m$ [27, 33, 38], $Fm\bar{3}m$ [37, 41], and $Ia\bar{3}d$ [42] symmetry. Although these organic-inorganic hybrid materials developed rapidly due to the commercial availability of surfactants as supramolecular templates and various (functional) organosilanes [2 – 4, 17, 18, 22, 43 – 58], binary surfactant mixtures or tailor-made surfactants were

Table 1. Synthesis details and important pore parameters of PMO materials under study.

Sample	Ratio of $C_{16\text{-}3\text{-}1}$ and $C_{16}TABr$[a]	Ratio[b] 10^{-3}	t_{aging} (h)	Product mesophase	a_s (BET) ($m^2\ g^{-1}$)[c]	$V_{p,des}$[d] ($cm^3\ g^{-1}$)	$d_{p,ads}$[e] (Å)	$d_{p,des}$[f] (Å)
1	0.91 : 0.00	6.79	24	cubic ($Fm\bar{3}m$)	583	0.45	30	27
2	0.55 : 0.00	6.79	24	cubic ($Fm\bar{3}m$)	656	0.57	30	28
3	0.55 : 0.00	7.02	24	cubic ($Fm\bar{3}m$)	584	0.53	30	30
4	0.55 : 0.00	6.69	24	cubic ($Fm\bar{3}m$)	634	0.55	30	30
5	0.00 : 0.91	6.79	24	hexagonal (*p6mm*)	750	0.61	27	26
6	0.00 : 0.55	6.69	24	hexagonal (*p6mm*)	758	0.59	27	26
7	0.00 : 0.55	7.37	24	hexagonal (*p6mm*)	689	0.48	27	24
8	0.455 : 0.455	6.79	24	cubic ($Fm\bar{3}m$)	725	0.56	30	28
9	0.182 : 0.728	6.79	24	cubic ($Pm\bar{3}n$)	784	0.64	30	28
10	0.182 : 0.728	7.74	24	hexagonal (*p6mm*)	474	0.34	26	26
11	0.182 : 0.728[g]	6.79	24	hexagonal (*p6mm*)	639	0.54	29	28
12	0.182 : 0.728[g]	6.79	24	hexagonal (*p6mm*)	739	0.66	30	29

[a] The ratio of binary surfactant, $C_{16\text{-}3\text{-}1}$ and $C_{16}TABr$, corresponding to 1 mol BTEE; [b] the molar ratio of NaOH to H_2O, corresponding to 1 mol BTEE; [c] specific BET surface area; [d] BJH desorption cumulative pore volume of pores between d_P = 15 Å and 200 Å; all samples were pretreated at 250 °C *in vacuo* until the pressure was $< 10^{-3}$ Torr; [e] pore diameter according to the maximum of the BJH pore size distribution calculated from the adsorption branch; [f] pore diameter according to the maximum of the BJH pore size distribution calculated from the desorption branch; [g] materials **11** and **12** were obtained with TMB as expander molecules, the molar ratio of TMB and BTEE was 1.0 and 1.5, respectively.

almost neglected [59–61]. Recently, we reported on the synthesis and characterization of face-centered cubic $Fm\bar{3}m$ PMOs by using divalent surfactant $C_{16\text{-}3\text{-}1}$ as an SDA under basic conditions [62, 63]. In this contribution, we wish to report the use of the divalent surfactant $C_{16\text{-}3\text{-}1}$ or binary surfactants (mixtures of $C_{16\text{-}3\text{-}1}$ and $C_{16}TABr$ with different molar ratios) as SDAs for controlling the formation of a series of highly ordered periodic mesoporous organosilicas in basic media. It will be shown that not only the surfactant type and binary surfactant molar ratio but also the base concentration and the presence of molecular expander molecules govern the formation of distinct mesophases.

Results and Discussion

PMO formation from either divalent or monocationic surfactant

Four PMO materials (**1**–**4**) were obtained by using different amounts of divalent surfactant $C_{16\text{-}3\text{-}1}$ as an SDA and BTEE as an organosilica source under slightly differing basic conditions (Table 1). The as-synthesized organosilicas show a cubic structure, as demonstrated by powder X-ray diffraction analysis (not shown). After removal of the surfactant, the peak intensity of the corresponding material increased (Fig. 1). Four well-resolved diffraction peaks are observed in the range of $1 < 2\theta < 4°$, that are indexed as (111), (200), (220), and (311) reflections. These patterns are in good accordance with

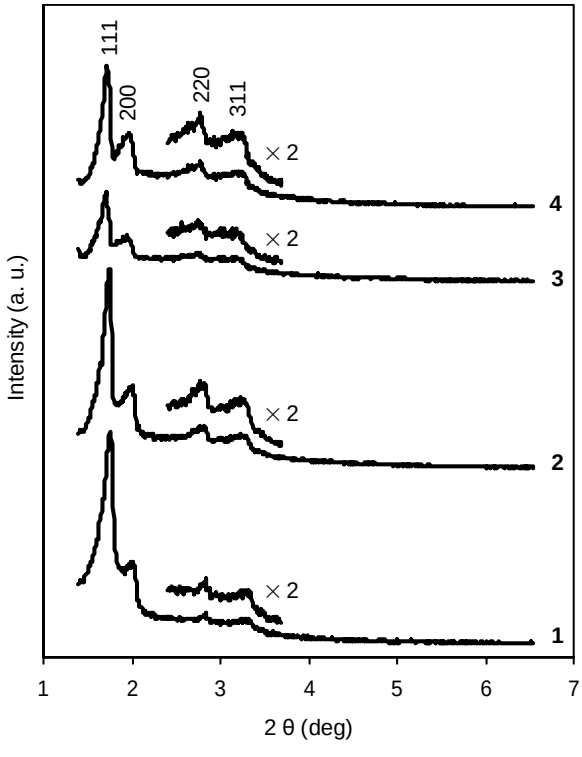

Fig. 1. Powder X-ray diffraction patterns of solvent-extracted samples **1**–**4**.

those of previously reported purely siliceous materials KIT-5 [64, 65], HOM-10 [66, 67], and periodic mesoporous organosilicas PMO[KIT-5] [62, 63] with a face-centered cubic $Fm\bar{3}m$ symmetry. PMO materi-

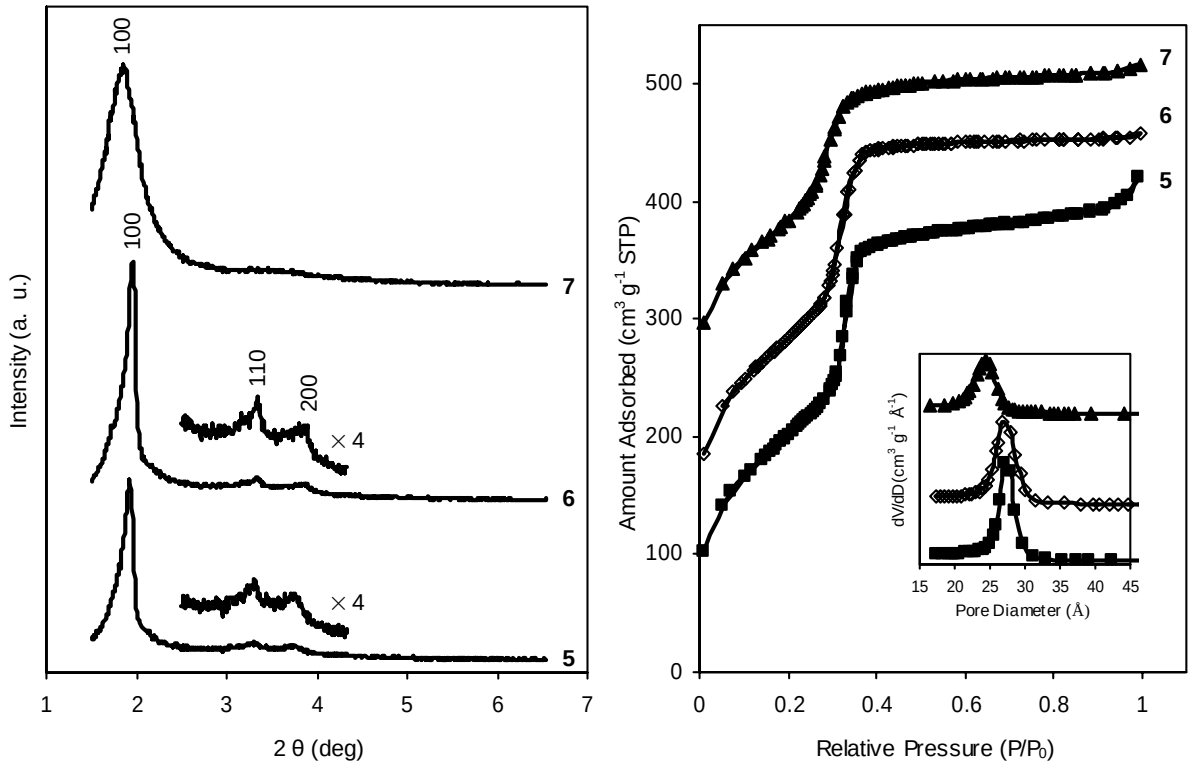

Fig. 2. Powder X-ray diffraction patterns of the solvent-extracted PMO samples **5** – **7** (left); N_2 physisorption isotherms of the solvent-extracted PMOs **5** – **7** (–■–: **5**; –◇–: **6**; –▲–: **7**); the inset shows the BJH pore size distribution from the adsorption branch (right).

als **2** – **4** obtained with lower surfactant concentration showed the diffraction peaks shifted to lower 2θ angles, however, the cubic mesophase was preserved. For comparison, using C_{16}TABr as an SDA under otherwise same synthesis conditions gave materials **5** – **7** with hexagonal *p6mm* symmetry. Their mesophase was also confirmed by powder X-ray diffraction analysis, as shown in Fig. 2 (left). These results imply that depending on the type of surfactant different organosilica mesophases are obtained. Commercially available C_{16}TABr or C_{16}TACl have been routinely employed for the synthesis of PMOs which often indicated 2D (*p6mm*) or 3D ($P6_3/mmc$) hexagonal structures and 3D ($Pm\bar{3}n$) cubic structures under basic conditions. To date, PMOs with $Fm\bar{3}m$ symmetry were obtained only by using divalent surfactant $C_{16\text{-}3\text{-}1}$ under basic conditions [62, 63] or the block copolymer Pluronic F127 as an SDA in the presence of inorganic salts in acidic media [41].

In order to accurately determine the space group of the various mesophases, transmission electron microscopy (TEM) analysis was carried out. For material **2**, the TEM images clearly indicate a high long-range ordering along the [100] and [110] directions (Figs. 3A and B). It is noteworthy that no intergrowths were observed along the [110] direction (which would belong to a 3D hexagonal phase), and only a regular cubic arrangement is emphasized by the view along the [100] direction. Also the absence of other cage-type mesoporous materials such as SBA-2 [68 – 70], SBA-12 [71], and FDU-1 type [72], gave further evidence of the purity of the cubic PMO materials with $Fm\bar{3}m$ symmetry. In addition, the "twinned" hexagonal-close-packed structure can also be ruled out, since the Fourier diffractograms corresponding to the images taken along [110] show no stacking faults and no streaking effects [69 – 71]. These results are in agreement with those of recently reported PMOs with space group $Fm\bar{3}m$ [62, 63]. However, the cubic $Fm\bar{3}m$ PMO obtained by using F127 as an SDA under acidic conditions indicated a remarkable intergrowth phenomenon [41]. For the hexagonal PMO **6**, TEM

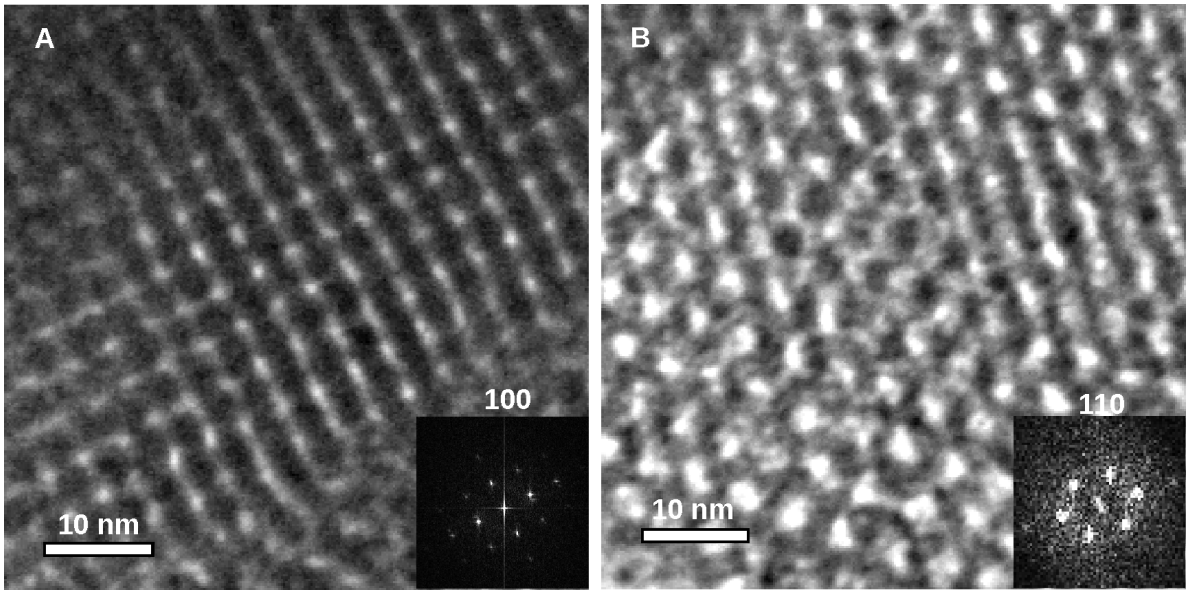

Fig. 3. Transmission electron microscopy images of the cubic PMO material **2** with $Fm\bar{3}m$ symmetry along A: [100] and B: [110], and their Fourier diffractograms.

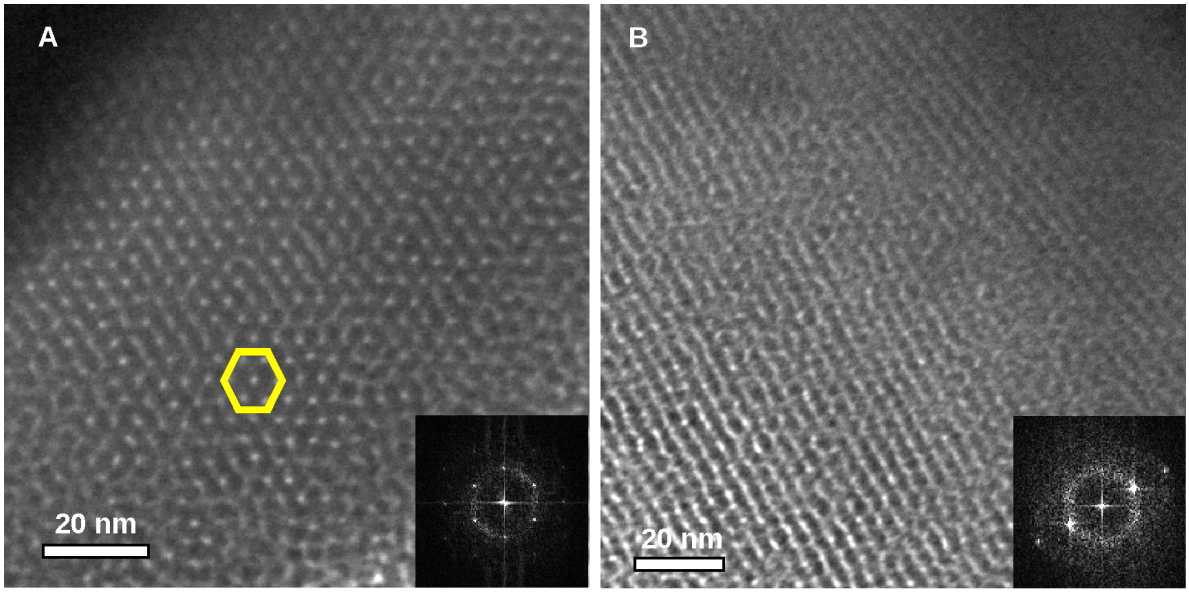

Fig. 4. TEM images for hexagonal PMO material **6** with *p6mm* symmetry viewed along the direction of the pore axis (A) and in the direction perpendicular to the pore axis (B); the Fourier diffractograms are also shown.

images along the direction of the pore axis and the direction perpendicular to the pore axis indicated good long-range ordering, revealing nice views of the channels and line arrays, respectively (Fig. 4).

The N_2 adsorption-desorption isotherms of materials **1**–**4** are of type IV with H2 hysteresis loops (Fig. 5, left). However, the shape of the isotherm is not completely similar to that of previously reported purely siliceous mesoporous materials KIT-5 [64, 65]. This is probably due to the fact that materials **1**–**4** feature small unit cell parameters ($\sim 88-89$ Å, calculated from $a = d_{111}(3)^{1/2}$) and small pore sizes (~ 30 Å).

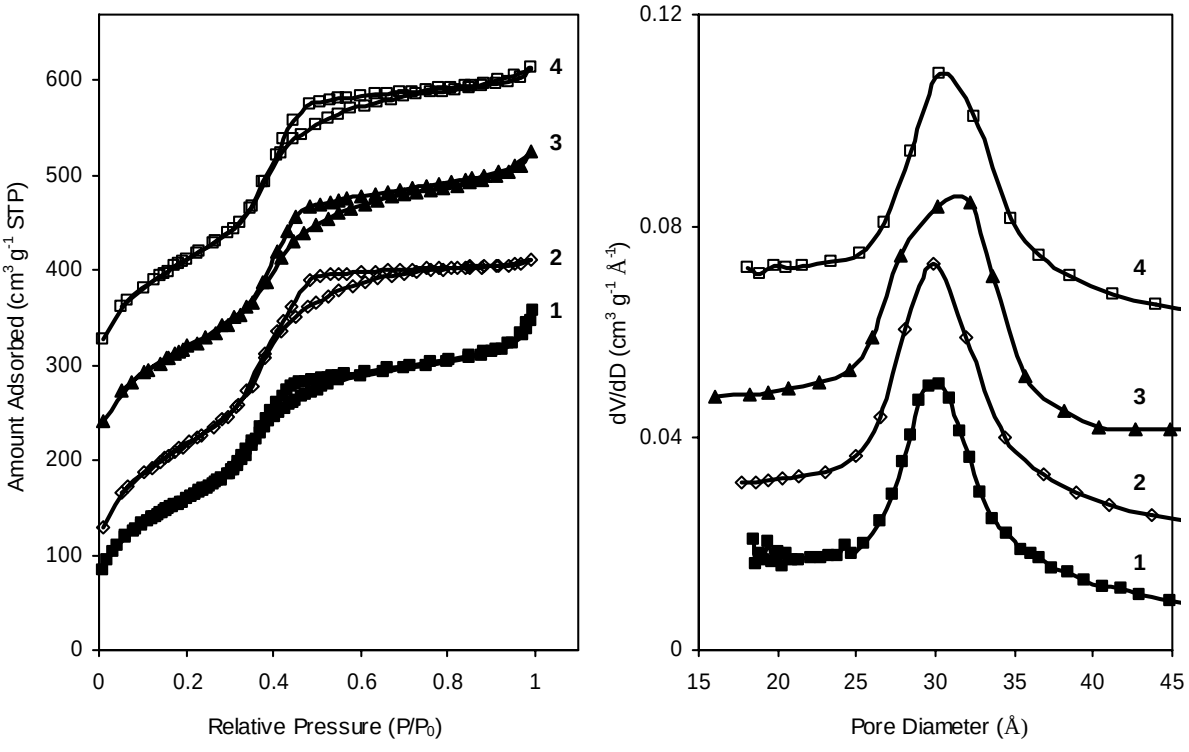

Fig. 5. N_2 physisorption isotherms of solvent-extracted PMO samples **1** – **4** (–■–: **1**; –◇–: **2**; –▲–: **3**–□–: **4**) (left); corresponding pore size distributions (BJH) calculated from the adsorption branch for samples **1** – **4** (right).

With a decrease of the divalent surfactant concentration, the BET surface area and pore volume generally increased, while the pore size distributions did not significantly change (Fig. 5, right). However, materials **5** – **7** obtained from C_{16}TABr as an SDA, exhibited type IV isotherms without hysteresis loops (Fig. 2, right), a narrow BJH (Barret Joyner Halenda) pore size distribution, overall smaller pores (Fig. 2, right, inset), and larger BET surface areas as compared to materials **1** – **4**. These findings implicate that divalent surfactants can considerably enlarge the pore diameter of PMOs compared to commercially available quaternary hexadecyltrimethylammonium bromide salt surfactants.

PMO mesophase control via mixtures of divalent surfactant $C_{16\text{-}3\text{-}1}$ and C_{16}TABr as SDAs

Using the same synthesis procedure, equimolar or unequimolar mixtures of the divalent surfactant $C_{16\text{-}3\text{-}1}$ and C_{16}TABr as SDAs produced materials **8** – **10**. When the total molar concentration of an equimolar binary surfactant mixture is 0.91 corresponding to 1 mol BTEE, material **8** with a face-centered cubic $Fm\bar{3}m$ symmetry is obtained, as demonstrated by powder X-ray diffraction (Fig. 6, left). Four well-resolved peaks were observed, which are indexed as (111), (200), (220), and (311) reflections, respectively. The ratios of different lattice *d* spacings from XRD patterns are in good agreement with the result of geometry calculations, corroborating the face-centered cubic structure of material **8**. Keeping the total binary surfactant concentration constant, a molar ratio of $C_{16\text{-}3\text{-}1}$ to C_{16}TABr of 0.25 gave material **9** displaying a cubic mesophase with $Pm\bar{3}n$ symmetry (Fig. 6, left). Three well-resolved peaks indexed as (200), (210), and (211) reflections are clearly observed, similar to those of previously reported mesoporous silicas [73, 74] or periodic mesoporous organosilicas [16, 23]. The cell parameter for solvent-extracted material **9** is about 110 Å. This result manifests that alteration of the molar ratio of the binary surfactant leads to the formation of periodic mesoporous organosilicas with different symmetry. This change of mesophases was also revealed by TEM analysis. Representative TEM images for PMOs **8** and **9** are shown in Figs. 7 and 8, respectively. Under the same synthesis conditions, however,

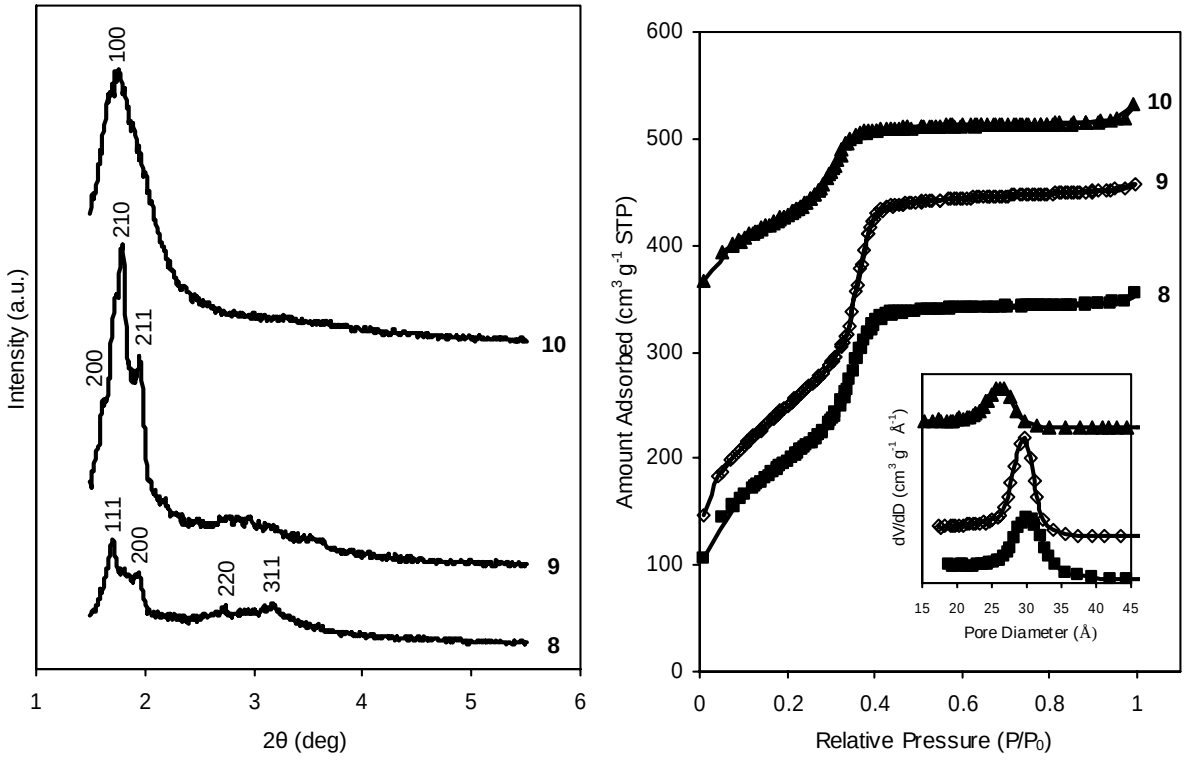

Fig. 6. Powder X-ray diffraction patterns of solvent-extracted PMO samples **8** – **10** (left); N_2 physisorption isotherms of solvent-extracted PMOs (–■–: **8**; –◇–: **9**; –▲–: **10**); the inset shows the BJH pore size distribution from the adsorption branch (right).

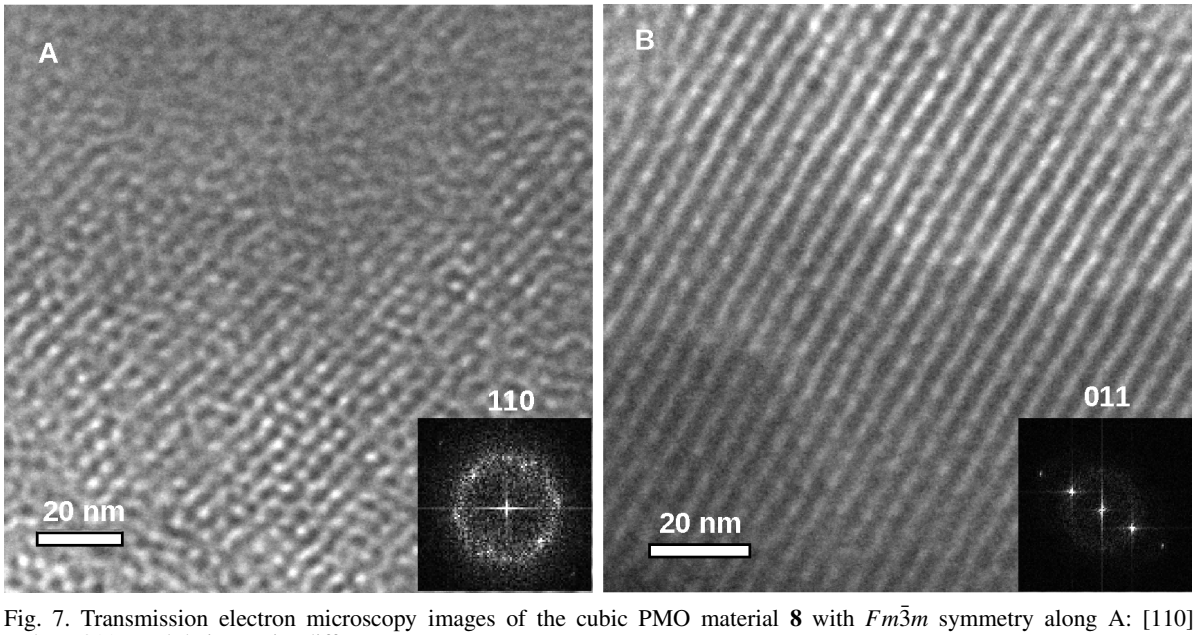

Fig. 7. Transmission electron microscopy images of the cubic PMO material **8** with $Fm\bar{3}m$ symmetry along A: [110] and B: [011], and their Fourier diffractograms.

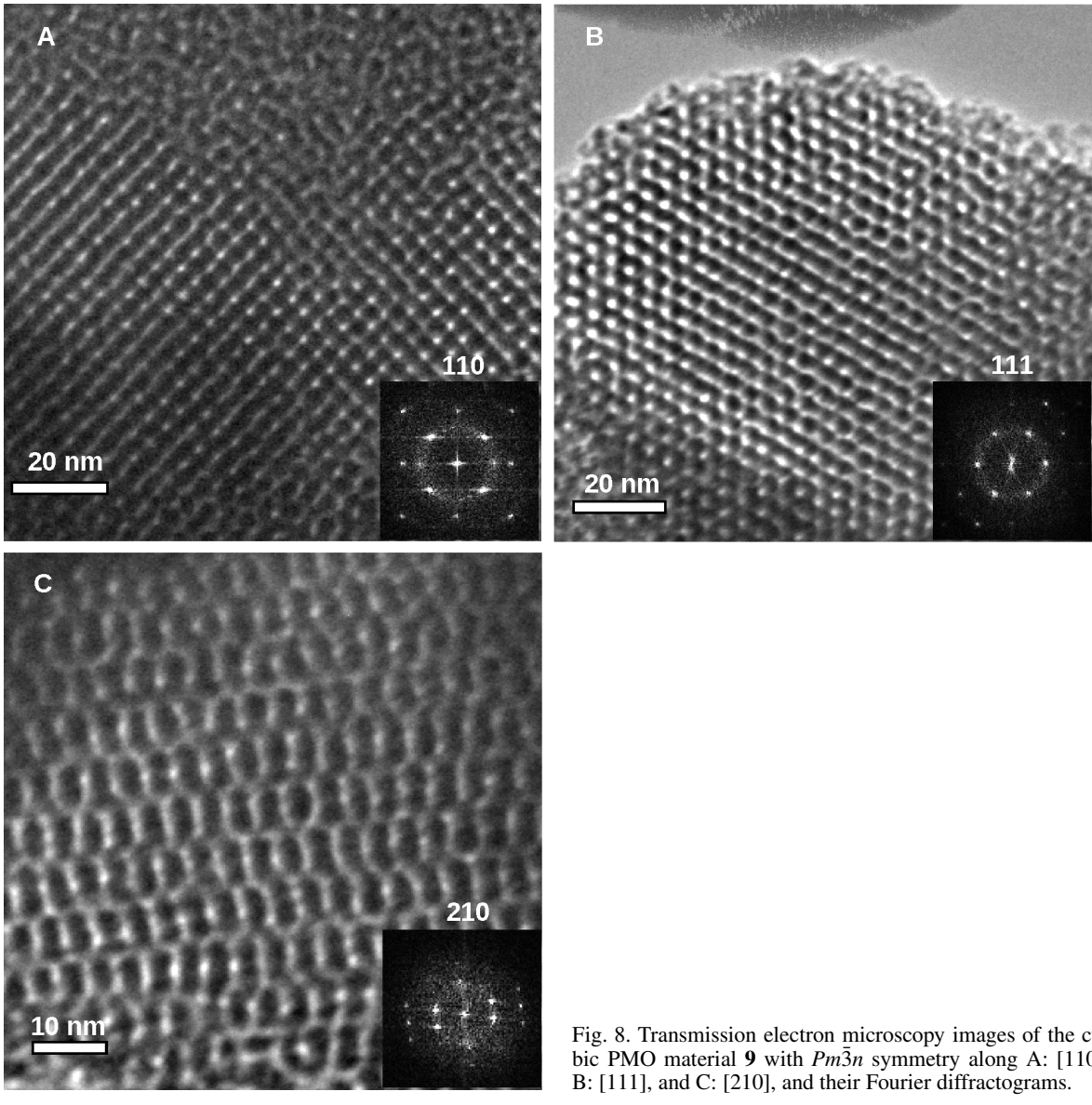

Fig. 8. Transmission electron microscopy images of the cubic PMO material **9** with $Pm\bar{3}n$ symmetry along A: [110], B: [111], and C: [210], and their Fourier diffractograms.

the increase of base concentration results in the formation of hexagonal mesoporous organosilica **10**. Its PXRD pattern shows only one diffraction peak indexed as (100) reflection (Fig. 6, left).

N_2 adsorption-desorption isotherms for materials **8** – **10** are of type IV without hysteresis loop (Fig. 6, right). The molar ratio of $C_{16\text{-}3\text{-}1}/C_{16}$TABr and the base concentration also affect the BET surface area ranging from 780 $m^2\,g^{-1}$ (**9**) to 470 $m^2\,g^{-1}$ (**10**). Material **9** has a larger pore volume (0.64 $cm^3\,g^{-1}$) compared to materials **8** (0.54 $cm^3\,g^{-1}$) and **10** (0.34 $cm^3\,g^{-1}$). Materials **8** – **10** display a narrow pore size distribution with the maxima centered at 30, 30, and 26 Å, respectively (Fig. 6, right).

^{13}C CP MAS and ^{29}Si MAS NMR studies

The ^{13}C cross-polarization (CP) MAS NMR spectrum of the solvent-extracted PMO material **2** shows a strong signal at 5.4 ppm (Fig. 9, left), confirming the bridging ethylene groups as the exclusive organic functionality, that is, a uniform $SiO_{1.5}$-CH_2-CH_2-$SiO_{1.5}$

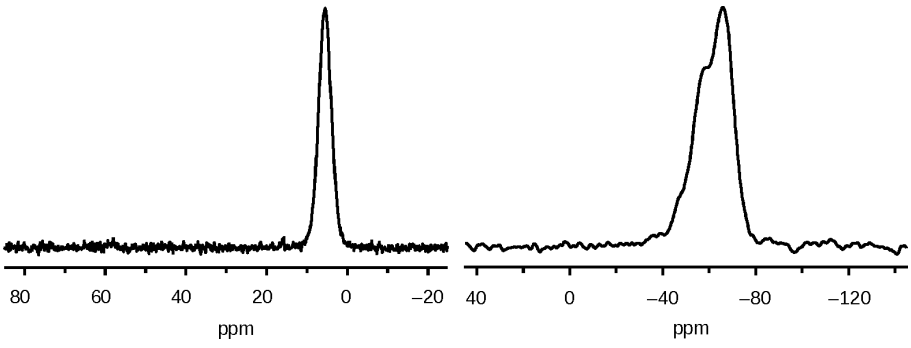

Fig. 9. ^{13}C CP MAS NMR (left) and ^{29}Si MAS NMR spectra (right) for the solvent-extracted PMO material **2**.

structural unit. Carbon signals assignable to surfactant molecules were not observed indicative of their complete removal from the mesoporous organosilicas. IR spectra also demonstrated this result, as for solvent-extracted PMO **2** the framework vibrations typical of these materials are displayed, comprising (i) Si–C stretching modes at 1270 cm^{-1}, (ii) a broad absorption band at 1000 – 1200 cm^{-1} indicative of Si–O–Si siloxane bonds, and (iii) bands at 770 and 720 cm^{-1} attributable to the symmetric Si–O stretching vibration are displayed.

The ^{29}Si MAS NMR spectra of the surfactant-free PMO **2** displayed two peaks at −57 and −67 ppm (Fig. 9, right), assignable to T^2 [$CSi(OSi)_2OH$)] and T^3 [$CSi(OSi)_3$] silicon resonances, respectively. This is in agreement with a condensed organic–inorganic network of composition $O_3Si–CH_2–CH_2–SiO_3$ and $(O_3Si–CH_2–CH_2)SiO_2(OH)$ surface sites. In addition, the absence of any Q^n [$Si(OSi)_n(OH)_{4-n}$] species revealed complete cross-linking *via* covalent Si–C bonds. This finding is in accordance with the framework structure of ethylene-silica materials synthesized in the presence of cationic quaternary ammonium surfactants [1, 16, 21, 23] or neutral alkylamine templates [30], corroborating that carbon-silicon bond cleavage does not occur during the basic hydrothermal treatment of precursors BTEE or in the process of surfactant-extraction from the as-synthesized mesoporous organosilica.

Influence of the synthesis parameters

In sol-gel multiphase synthesis systems, due to the complexity of the reaction process, changes of any synthesis parameter can result in the formation of new mesophase structures. In general, type, structure and concentration of surfactant, pH value of the reaction system, counterions, reaction temperature, co-solvent or organic additives often influence the structure of mesoporous materials. In fact, the formation of the final ordered periodic mesophase is a result of a synergistic interaction between the surfactant template and the organosilica component. Previous studies also emphasized this point [75]. Consequently, the following discussion puts emphasis on the various factors governing mesophase formation.

Effect of the surfactant

It is well-known that, in the process of mesoporous materials synthesis, type, chain length, and charge of the surfactant often effectively affect the mesophase structure. Huo *et al.* [76] have proposed that the structure of mesoporous silicas can be rationalized on the basis of the surfactant packing parameter g ($= V/(a_0 l)$), where V is the total volume of the surfactant chains plus any co-solvent organic molecule between the chains, a_0 is the effective hydrophilic headgroup area at the micelle interface, and l is the kinetic surfactant tail length or the curvature elastic energy. This value g is defined by two factors, namely charge matching at the interface headgroup-organosilica and packing of carbon chains. The former is controlled by the pH value, the co-solvent, and the counterions, while the latter is affected by the reaction temperature and the organic additives. In our reaction system, a remarkable effect of the surfactant is observed. Applying the same surfactant concentrations, it is only the use of the divalent surfactant $C_{16\text{-}3\text{-}1}$ instead of routine surfactant C_{16}TABr as micellar template, which changes the mesophase from hexagonal *p6mm* to cubic $Fm\bar{3}m$ symmetry, *i. e.*, materials **1** *versus* **5**. For previously reported purely siliceous mesophases, investigations with divalent surfactants as SDAs under basic conditions often indicated the formation of a 3D

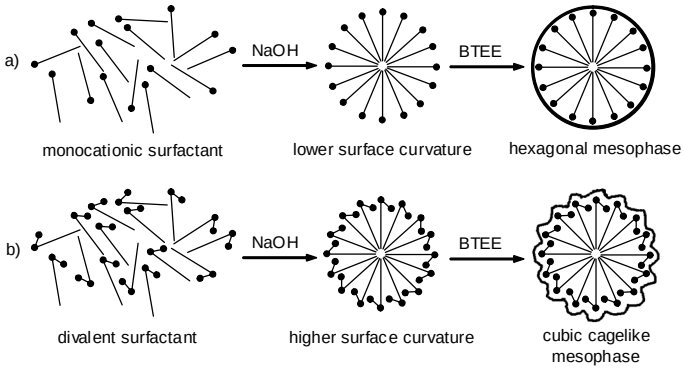

Scheme 1. Possible scenario of the formation of different mesophases using various surfactants as templates.

cage-like hexagonal structure (space group $P6_3mmc$) [68 – 70, 76, 77]. Noteworthy, highly ordered periodic mesoporous silicas with cubic $Fm\bar{3}m$ symmetry can be obtained under acidic conditions. However, when divalent surfactants as a micelle template are applied for PMO synthesis, a change of the divalent surfactant concentration gave PMOs exhibiting three different symmetries with space group $Pm\bar{3}n$, or $Fm\bar{3}m$, or $p6mm$ [62, 63]. This result can be explained likewise with charge matching between the divalent surfactant molecules and the organosilica component and the type of divalent surfactant including carbon chain length and structure. We know that the hydrolyzed product of the bridged organosilica precursor BTEE displays a lower charge density than that of TEOS, and in order to maintain charge density balance at the interface, divalent cationic surfactants favor a high surface curvature meaning a larger value a_0, and hence, a smaller value g. When organosilica condensation proceeds, the surface curvature will increase which is reflected by a mesophase transformation from hexagonal ($p6mm$) to cubic ($Fm\bar{3}m$) symmetry. Our previous report also revealed a similar trend for C_{18}TABr (low surface curvature) and C_{18-3-1} (high surface curvature) as SDAs [78]. A simple model for the supramolecular templating of different mesophases with such surfactants is hypothesized in Scheme 1. In addition, the molar ratio of the binary surfactant mixture is also known to influence the packing structure of the micellar template and results in the formation of distinct mesophases. Correspondingly, high ratios of monocationic surfactant and divalent surfactant or when a monocationic surfactant is mixed with a small amount of divalent surfactant does not result in a mesophase transformation, that is, the prevailing surfactant will determine the packing structure, and hence, the final mesophase [78].

Effect of the base concentration

Samples **9** and **10** obtained by using the same binary surfactant concentration, however, a different amount of NaOH indicated a distinct change of the mesophase structure. A relatively high base concentration (PMO **10**) resulted in the formation of a hexagonal mesophase. This can be attributed to that NaOH influences the packing structure of the binary surfactant. Deprotonation of the multihydroxyl organosilica component is enhanced by a higher base concentration, and the higher overall negative charge will require additional cationic surfactants as a charge balance. Since the concentration of the surfactant is constant in the synthesis system, charge balance between the surfactant and the organosilica composite is kept only upon further condensation of the deprotonated organosilica species, thus forming a higher surface curvature. However, if the base concentration is increased continuously, the balance cannot be met, and the binary surfactant composite separates and reorganizes to form lower-surface curvatural packing structures. This latter scenario is documented by the formation of disorderd cubic or hexagonal mesophases in our binary surfactant system. The obtained materials often exhibit broad PXRD patterns such as material **10**. Recent studies revealed that the change of base concentration in binary surfactant systems leads to mesophase transformations from primitive cubic $Pm\bar{3}n$ to face-centered cubic $Fm\bar{3}m$, distorted cubic and finally MSU-type wormhole-like mesophases [79]. These findings can be also interpreted with charge-matching phenomena.

Co-solvent effect

Organic additives such as co-surfactants or expander molecules have been studied in detail with respect to the synthesis of mesoporous silicas and mesoporous

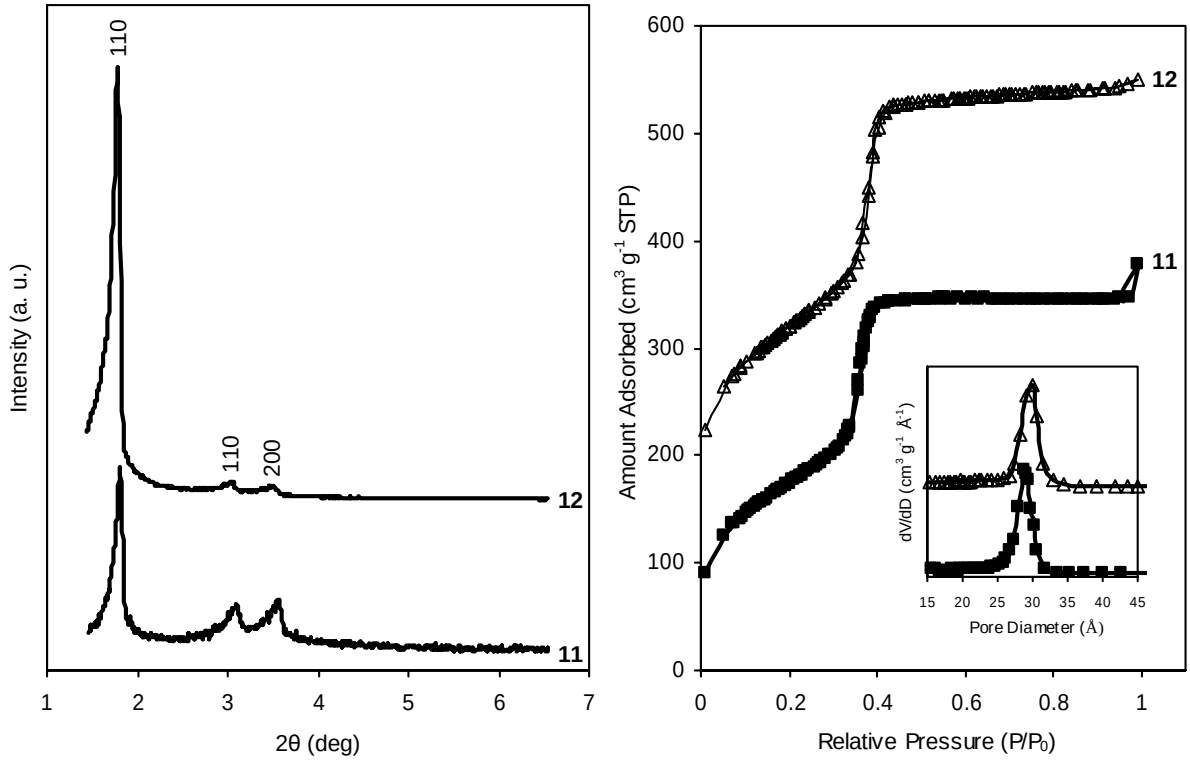

Fig. 10. Powder X-ray diffraction patterns of solvent-extracted PMO samples **11** and **12** (left); N_2 physisorption isotherms of solvent-extracted PMOs **11** and **12** (–■–: **11**; –△–: **12**); the inset shows the corresponding BJH pore size distribution from the adsorption branch (right).

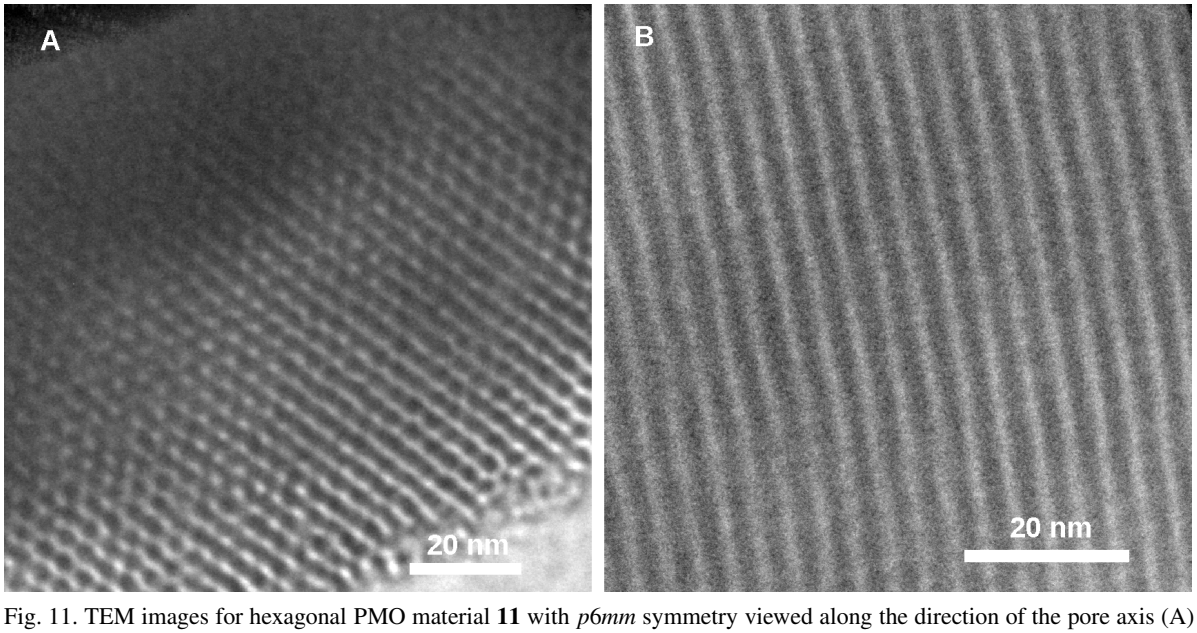

Fig. 11. TEM images for hexagonal PMO material **11** with *p6mm* symmetry viewed along the direction of the pore axis (A) and in the direction perpendicular to the pore axis (B).

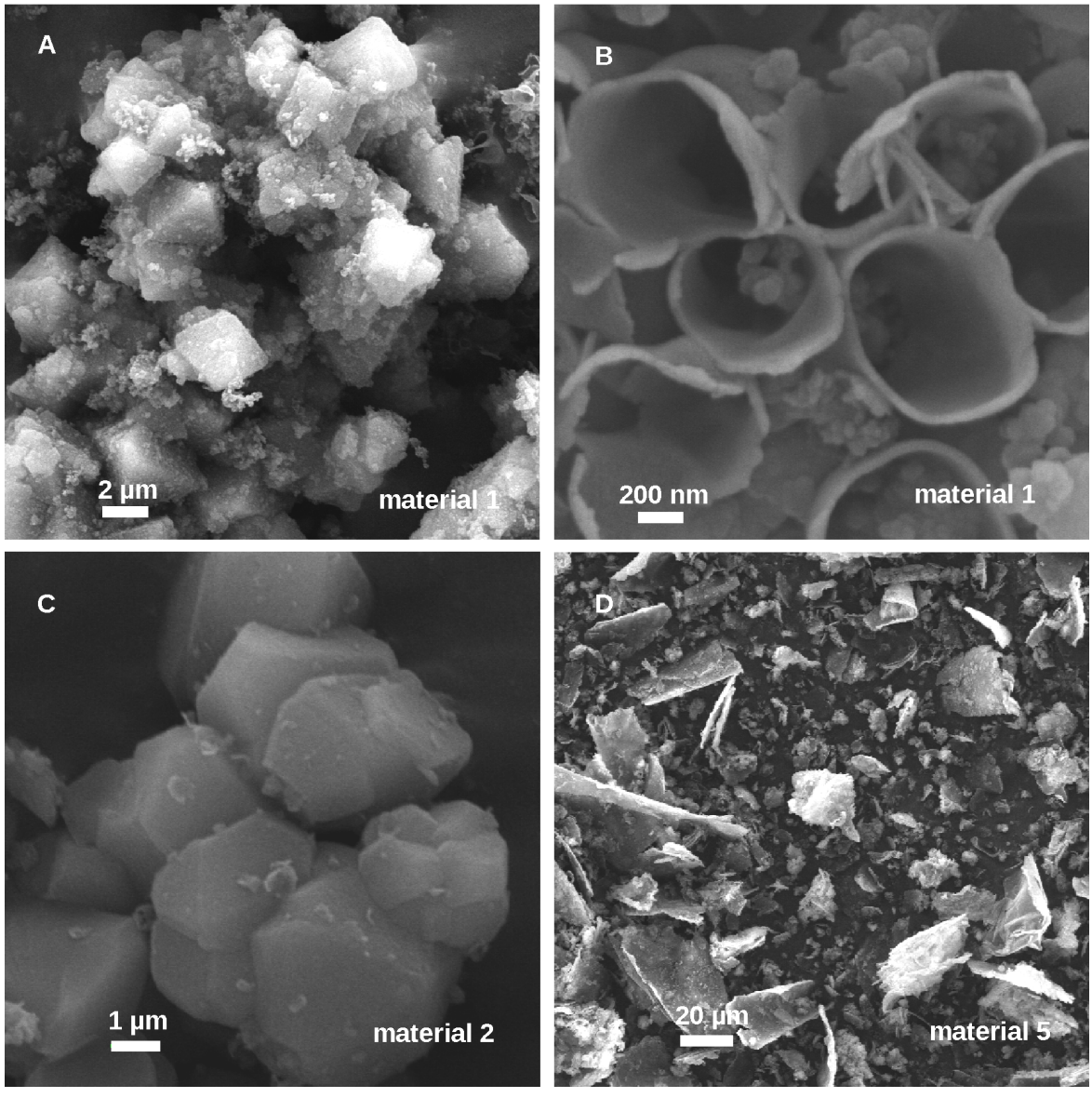

Fig. 12. Scanning electron micrographs for materials **1** (A, B), **2** (C), and **5** (D).

organosilicas [34, 80, 81]. These organic components can effectively enlarge the pore size [34, 80 – 82, 83], control topology of material [84], affect the micelle formation [85], and promote phase transformations [86 – 89]. In our system, mesophase transformation occurred in the presence of TMB (1,3,5-trimetylbenzene = mesitylene) as an expander molecule. Materials **11** and **12** were obtained by the procedure used for material **9**, with the addition of different molar amounts of TMB as the only alteration. The obtained materials **11** and **12** exhibit a hexagonal mesophase, which was confirmed by powder X-ray diffractions, as shown in Fig. 10 (left). Three well-resolved peaks indexed as (100), (110), and (200) reflections are observed, indicative of a typical hexagonal *p6mm* symmetry. TEM analysis corroborated highly ordered hexagonal mesopore arrays of material **11** (Fig. 11).

N_2 gas physisorption isotherms of materials **11** and **12** (Fig. 10, right) revealed a decreased BET surface area and a pore volume comparable with those of

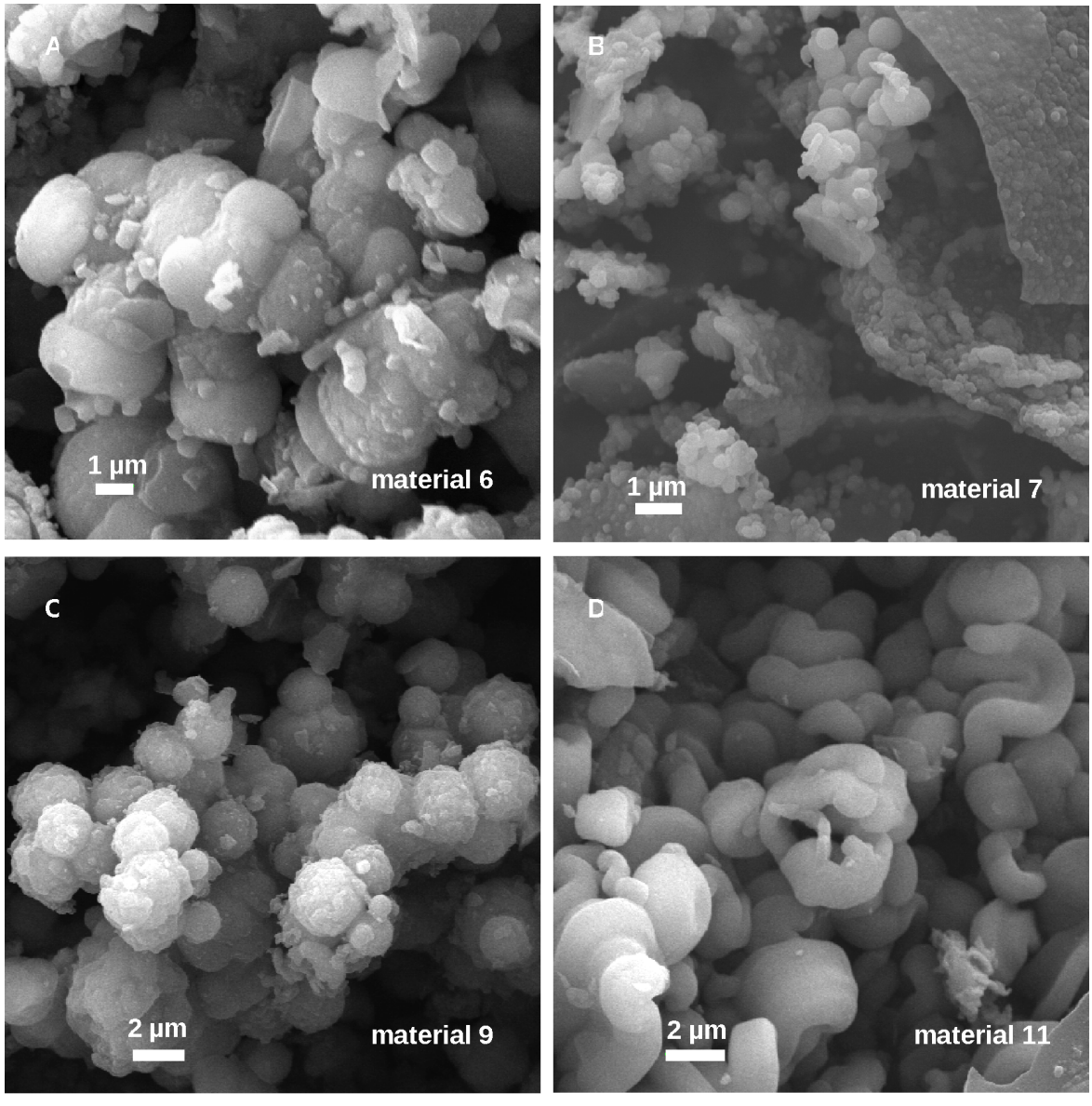

Fig. 13. Scanning electron micrographs for materials **6** (A), **7** (B), **9** (C), and **11** (D).

material **9**. With increase of the amount of TMB, the BET surface area and pore volume increased while the pore size enlarged slightly. These findings demonstrate that the organic molecule TMB can be assigned a dual role as a co-solvent as well as an expander molecule. We suggest that a small amount of TMB is distributed uniformly between the surfactant molecules, thus decreasing the surfactant curvature, which results in the formation of a hexagonal mesophase. When larger amounts of TMB are added, parts of the TMB molecules are dispersed into the binary surfactant micelle as fillers thereby changing the surface curvature, while others act as expanders causing the binary surfactant-composite micelle to reconstruct and to form a rod-shaped micelle with a TMB core. Then, the organosilica composite has to reorganize around the rod-shaped micelle for reasons of charge balance, forming a hexagonal mesophase. As another result, the

pore diameter of the obtained material gets enlarged. These findings are in accordance with previous reports on the use of different binary surfactants as templates. There, we have shown that addition of TMB to a cubic PMO synthesis system caused mesophase transformation from cubic $Pm\bar{3}n$ to hexagonal *p6mm* symmetry [78].

Scanning electron microscopy (SEM)

Scanning electron microscopy (SEM) images revealed that different synthesis conditions result in distinct morphologies of the PMO materials (Figs. 12 – 13). The face-centered cubic PMO material **1** obtained by using the divalent surfactant as a template consists of pyramid-like, broken hollow spheres accompanied by small spherical aggregations (Figs. 12A and B). PMO **2** is composed of irregular bulk particles (Fig. 12C). When monocationic surfactant C_{16}TABr was used as a structure-directing agent, the obtained materials **5** – **7** with hexagonal symmetry display bark-like (Fig. 12D), ellipsoid-like aggregations (Fig. 13A), and spherical or tabular shapes (Fig. 13B), respectively. A mixture of divalent $C_{16\text{-}3\text{-}1}$ and C_{16}TABr produced mesophase **8**, which contains discoidal or lamellar particles (not shown). The cubic $Pm\bar{3}n$ PMO **9** features uniformly sized spherical morphologies with coarse external surfaces (Fig. 13C), while the hexagonal PMO **11** consists of rope-like aggregations (Fig. 13D).

Conclusion

Highly ordered periodic mesoporous organosilica materials with hexagonal or cubic structure can be fabricated by carefully controlling the synthesis parameters. Particularly, variation of the surfactant type is a viable strategy to accomplish mesophase transformations in basic media. Accordingly, face-centered cubic $Fm\bar{3}m$ mesoporous organosilicas were obtained by using divalent surfactant $C_{16\text{-}3\text{-}1}$ or equimolar mixtures of divalent $C_{16\text{-}3\text{-}1}$ and C_{16}TABr. Cubic PMOs with $Pm\bar{3}n$ symmetry result from special mixtures of divalent surfactant $C_{16\text{-}3\text{-}1}$ and C_{16}TABr. Hexagonal PMOs with *p6mm* symmetry generally formed in the presence of a single-component monocationic surfactant, however, also from binary surfactant mixtures after addition of the expander molecule TMB. Furthermore, the molar ratio of NaOH and H_2O, the molar ratio of binary surfactant mixtures, and the addition of a co-solvent markedly influence the structure and physical properties of the PMO mesophases. For example, under otherwise identical synthesis conditions, a decrease of the NaOH concentration implied a mesophase transformation from *p6mm* to $Pm\bar{3}n$ symmetry. These studies clearly demonstrate that the formation of different mesophases depends mainly on the surfactant packing structure.

Experimental Section

1,2-Bis(triethoxysilyl)ethane (BTEE) from Aldrich as silica precursor, hexadecyltrimethylammonium bromide (C_{16}TABr) as SDA, mesitylene (TMB) as expander molecule from Fluka, and sodium hydroxide from Merck-Schuchardt were used as received. Divalent surfactant *N*-(3-trimethylammoniumpropyl)hexadecylammonium dibromide, $[CH_3(CH_2)_{15}NMe_2(CH_2)_3NMe_3]^{2+}$ $2Br^-$ ($C_{16\text{-}3\text{-}1}$), was synthesized by reaction of hexadecyldimethylamine with (3-bromopropyl)trimethylammonium bromide.

*Synthesis of PMOs **1** – **7** using divalent surfactants $C_{16\text{-}3\text{-}1}$ or C_{16}TABr as SDAs*

A typical synthesis is as follows (material **1**): A mixture of $C_{16\text{-}3\text{-}1}$ (2.42 g, 4.56 mmol) and NaOH (0.46 g, 11.5 mmol) in warm deionized water (30.27 g, 1.682 mol) was stirred at ambient temperature to form a clear solution. BTEE (1.83 g, 5.01 mmol) was added under vigorous stirring, and the stirring was continued for 24 h at ambient temperature to give a homogeneous solution. Heating this solution to 95 °C for 6 h brought about a white precipitation. Finally, the suspension was transferred into a polypropylene bottle to age at 95 °C for 24 h. The final molar composition of the gel was 1 BTEE : 0.91 $C_{16\text{-}3\text{-}1}$: 2.28 NaOH : 336 H_2O. The resulting white precipitate was recovered by suction filtration before cooling without water washing, and dried in air. Synthesis of materials **2** – **7** is similar to that of material **1**. Detailed synthesis parameters are listed in Table 1.

*Synthesis of PMOs **8** – **12** using mixtures of binary surfactants $C_{16\text{-}3\text{-}1}$ and C_{16}TABr as SDAs*

A typical synthesis is as follows (material **8**): A mixture of $C_{16\text{-}3\text{-}1}$ (2.42 g, 4.56 mmol), C_{16}TABr (1.66 g, 4.55 mmol), and NaOH (0.91 g, 22.75 mmol) in warm deionized water (60.55 g, 3.360 mol) was stirred at ambient temperature to form a clear solution. The BTEE (3.66 g, 10.01 mmol) was added under vigorous stirring conditions, and the stirring was continued for 24 h at ambient temperature to afford a homogeneous solution. Heating this solution to 95 °C for 6 h brought about a white precipitation. Finally, the suspension was aged at 95 °C for 24 h in a polypropylene bottle. The final molar composition of the gel was 1 BTEE : 0.455

$C_{16\text{-}3\text{-}1}$: 0.455 C_{16}TABr : 2.28 NaOH : 336 H_2O. The resulting white product was recovered by suction filtration before cooling, and dried at ambient temperature. Samples **9** and **10** were prepared by using the same method, only changing the molar ratio of the binary surfactant mixture, or the base concentration. For the synthesis of mesoporous organosilicas **11** and **12**, mesitylene as an expander molecule was added to the reaction mixture under stirring after the binary surfactant had completely dissolved in warm deionized water. Upon formation of a clear solution, BTEE as the organosilica precursor was added to the surfactant solution, and the procedure continued as described above (Table 1).

Surfactant removal

For all of the materials, the surfactant was removed by two steps. A typical extraction process was as follows. *Ca.* 1.0 g of a mesoporous organosilica material was stirred in ethanol (250 mL) and hydrochloric acidic (37 %, 5 g) solution at 50 $\sim$ 60 °C for 6 h, the precipitate was separated by suction filtration and dried in air. Then the retained surfactant was further extracted in hydrochloride-acidified ethanol solution for 24 h by using a Soxhlet apparatus.

Characterization

The powder X-ray diffraction (PXRD) patterns of PMOs were collected on a Philips X'pert PRO diffractometer using monochromatic CuK_α (λ = 1.5418 Å) radiation. The diffractograms were recorded in the 2θ range of 0.50 – 9.99° in the step/scan mode (step width: 0.0086, accumulation time: 54.61 s step^{-1}). Transmission electron micrographs (TEM) were obtained using a Jeol JEM2100 instrument operated at 160 kV. A representative sample was dispersed in ethanol (99.9 %) using the ultrasonic method and loaded onto a copper micro grid. Scanning electron microscopy (SEM) images were recorded on a Jeol JSM-5900LV microscope operated at an accelerating voltage of 10 – 20 kV. SEM images reported here are representative of the corresponding material. FT-IR spectra of dehydrated organosilicas were recorded on a Perkin Elmer FT-IR spectrometer 1760X using Nujol mulls sandwiched between CsI plates. ^{13}C and ^{29}Si MAS NMR spectra were obtained at ambient temperature on a Bruker AV300 instrument in a magnetic field of 7.04 T by using 4 mm (^{13}C) and 7 mm (^{29}Si) standard MAS probes. The ^{13}C spectra were recorded using cross polarization and proton decoupling and referenced to adamantane (δ^{13}C: 28.46 and 37.85 ppm). The ^{29}Si NMR spectra referenced to Si[Si(CH$_3$)$_3$]$_4$ (δ^{29}Si: −9.8 ppm) were obtained by the application of single-pulse excitation with high-power proton decoupling at a spinning speed of 7 kHz. Nitrogen gas adsorption/desorption isotherms were measured at 77.4 K on an ASAP 2020 volumetric adsorption apparatus (Micromeritics) for relative pressures from 10^{-2} to 0.99 [a_m(N_2, 77 K) = 0.162 nm^2]. Prior to analysis the samples were degassed in the degas port of the adsorption analyzer at 523 K *in vacuo* for at least 4 h. The BET specific surface area was obtained from the nitrogen adsorption branch of the isotherm in the relative pressure range from 0.04 to 0.2 [90, 91]. The pore size distributions were calculated from the adsorption branches using the BJH method [92].

Acknowledgements

This work was supported by the Deutsche Forschungsgemeinschaft and the NANOSCIENCE program of the University of Bergen. Authors also gratefully acknowledge Dr. G. Raudaschl-Sieber for recording the solid-state NMR spectra.

[1] S. Inagaki, S. Guan, Y. Fukushima, T. Ohsuna, O. Terasaki, *J. Am. Chem. Soc*. **1999**, *121*, 9611 – 9614.
[2] C. Yoshina-Ishii, T. Asefa, N. Coombs, M. J. MacLachlan, G. A. Ozin, *Chem. Commun*. **1999**, 2539 – 2540.
[3] T. Asefa, M. J. MacLachlan, N. Coombs, G. A. Ozin, *Nature* **1999**, *402*, 867 – 871.
[4] B. J. Melde, B. T. Holland, C. F. Blanford, A. Stein, *Chem. Mater*. **1999**, *11*, 3302 – 3308.
[5] T. Tani, N. Mizoshita, S. Inagaki, *J. Mater. Chem*. **2009**, *19*, 4451 – 4456.
[6] S. Inagaki, O. Ohtani, Y. Goto, K. Okamoto, M. Ikai, K. Yamanaka, T. Tani, T. Okada, *Angew. Chem.* **2009**, *121*, 4102 – 4106; *Angew. Chem. Int. Ed.* **2009**, *48*, 4042 – 4046.
[7] N. Mizoshita, Y. Goto, M. P. Kapoor, T. Shimada, T. Tani, S. Inagaki, *Chem. Eur. J.* **2009**, *15*, 219 – 226.
[8] Y. Goto, N. Mizoshida, O. Ohtani, T. Okada, T. Shimada, T. Tani, S. Inagaki, *Chem. Mater*. **2008**, *20*, 4495 – 4498.
[9] V. Rebbin, R. Schmidt, M. Fröba, *Angew. Chem.* **2006**, *118*, 5335 – 5339; *Angew. Chem. Int. Ed.* **2006**, *45*, 5210 – 5214.
[10] S. Polarz, A. Kuschel, *Adv. Mater*. **2006**, *18*, 1206 – 1209.
[11] X. Meng, T. Yokoi, D. Lu, T. Tatsumi, *Angew. Chem.* **2007**, *119*, 7942 – 7944; *Angew. Chem. Int. Ed*. **2007**, *46*, 7796 – 7798.
[12] J. Morell, S. Chatterjee, P. J. Klar, D. Mauder, I. Shenderovich, F. Hoffmann, M. Fröba, *Chem. Eur. J.* **2008**, *14*, 5935 – 5940.
[13] S. MacQuarrie, M. P. Thompson, A. Blanc, N. J. Mosey, R. P. Lemieux, C. M. Crudden, *J. Am. Chem. Soc*. **2008**, *130*, 14099 – 14101.
[14] F. Hoffmann, M. Cornelius, J. Morell, M. Fröba, *Angew. Chem.* **2006**, *118*, 3290 – 3328; *Angew. Chem. Int. Ed*. **2006**, *45*, 3216 – 3251.
[15] Q. Yang, J. Liu, L. Zhang, C. Li, *J. Mater. Chem*. **2009**, *19*, 1945 – 1955.

[16] S. Guan, S. Inagaki, T. Ohsuna, O. Terasaki, *J. Am. Chem. Soc*. **2000**, *122*, 5660 – 5665.

[17] T. Asefa, M. J. MacLachlan, H. Grondey, N. Coombs, G. A. Ozin, *Angew. Chem.* **2000**, *112*, 1878 – 1881; *Angew. Chem. Int. Ed*. **2000**, *39*, 1808 – 1811.

[18] T. Asefa, C. Yoshina-Ishii, M. J. MacLachlan, G. A. Ozin, *J. Mater. Chem*. **2000**, *10*, 1751 – 1755.

[19] M. J. MacLachlan, T. Asefa, G. A. Ozin, *Chem. Eur. J*. **2000**, *6*, 2507 – 2511.

[20] M. Kruk, M. Jaroniec, S. Guan, S. Inagaki, *J. Phys. Chem. B* **2001**, *105*, 681 – 689.

[21] S. Hamoudi, Y. Yang, I. L. Moudrakovski, S. Lang, A. Sayari, *J. Phys. Chem. B* **2001**, *105*, 9118 – 9123.

[22] T. Asefa, M. Kruk, M. J. MacLachlan, N. Coombs, H. Grondey, M. Jaroniec, G. A. Ozin, *J. Am. Chem. Soc*. **2001**, *123*, 8520 – 8530.

[23] A. Sayari, S. Hamoudi, Y. Yang, I. L. Moudrakovski, J. R. Ripmeester, *Chem. Mater*. **2000**, *12*, 3857 – 3863.

[24] S. Inagaki, S. Guan, T. Ohsuna, O. Terasaki, *Nature* **2002**, *416*, 304 – 307.

[25] M. Kuroki, T. Asefa, W. Whitnal, M. Kruk, C. Yoshina-Ishii, M. Jaroniec, G. A. Ozin, *J. Am. Chem. Soc.* **2002**, *124*, 13886 – 13895.

[26] Y. Xia, Z. Yang, R. Mokaya, *Chem. Mater*. **2006**, *18*,1141 – 1148.

[27] A. Keilbach, M. Döblinger, R. Köhn, H. Amenitsch, T. Bein, *Chem. Eur. J*. **2009**, *15*, 6645 – 6650.

[28] H. Fan, Y. Lu, A. Stump, S. T. Reed, T. Baer, R. Schunk, V. Perez-Luna, G. P. López, C. J. Brinker, *Nature* **2000**, *405*, 56 – 60.

[29] Y. Lu, H. Fan, N. Doke, D. A. Loy, R. A. Assink, D. A. LaVan, C. J. Brinker, *J. Am. Chem. Soc*. **2000**, *122*, 5258 – 5261.

[30] M. D. McInall, J. Scott, L. Mercier, P. J. Kooyman, *Chem. Commun*. **2001**, 2282 – 2283.

[31] O. Muth, C. Schellbach, M. Fröba, *Chem. Commun*. **2001**, 2032 – 2033.

[32] H. Zhu, D. J. Jones, J. Zajac, J. Rozière, R. Dutartre, *Chem. Commun*. **2001**, 2568 – 2569.

[33] E.-B. Cho, K.-W. Kwon, K. Char, *Chem. Mater*. **2001**, *13*, 3837 – 3839.

[34] M. C. Burleigh, M. A. Markowitz, E. M. Wong, J.-S. Lin, B. P. Gaber, *Chem. Mater*. **2001**, *13*, 4411 – 4412.

[35] A. Sayari, Y. Yang, *Chem. Commun*. **2002**, 2582 – 2583.

[36] S. Hamoudi, S. Kaliaguine, *Chem. Commun*. **2002**, 2118 – 2119.

[37] J. R. Matos, M. Kruk, L. P. Mercuri, M. Jaroniec, T. Asefa, N. Coombs, G. A. Ozin, T. Kamiyama, O. Terasaki, *Chem. Mater*. **2002**, *14*, 1903 – 1905.

[38] W. Guo, I. Kim, C.-S. Ha, *Chem. Commun*. **2003**, 2692 – 2693.

[39] X. Y. Bao, X. S. Zhao, X. Li, P. A. Chia, J. Li, *J. Phys. Chem. B* **2004**, *108*, 4684 – 4689.

[40] X. Y. Bao, X. S. Zhao, *J. Phys. Chem. B* **2005**, *109*, 10727 – 10736.

[41] L. Zhao, G. Zhu, D. Zhang, Y. Di, Y. Chen, O. Terasaki, S. Qiu, *J. Phys. Chem. B* **2005**, *109*, 764 – 768.

[42] Z. Zhang, X. Yan, B. Tian, S. Shen, D. Chen, G. Zhu, S. Qiu, D. Zhao, *Chem. Lett*. **2005**, *34*, 182 – 183.

[43] H. Zhu, D. J. Jones, J. Zajac, R. Dutartre, M. Rhomari, J. Rozière, *Chem. Mater*. **2002**, *14*, 4886 – 4894.

[44] C. Baleizão, B. Gigante, D. Das, M. Alvaro, H. Garcia, A. Corma, *Chem. Commun*. **2003**, 1860 – 1861.

[45] K. Landskron, B. D. Hatton, D. D. Perovic, G. A. Ozin, *Science* **2003**, *302*, 266 – 269

[46] B. Hatton, K. Landskron, W. Whitnall, D. Perovic, G. A. Ozin, *Acc. Chem. Res*. **2005**, *38*, 305 – 312.

[47] K. Landskron, G. A. Ozin, *Angew. Chem.* **2005**, *117*, 2145 – 2147; *Angew. Chem. Int. Ed*. **2005**, *44*, 2107 – 2109.

[48] M. C. Burleigh, S. Jayasundera, M. S. Spector, C. W. Thomas, M. A. Markowitz, B. P. Gaber, *Chem. Mater.* **2004**, *16*, 3 – 5.

[49] O. Olkhovyk, M. Jaroniec, *J. Am. Chem. Soc*. **2005**, *127*, 60 – 61.

[50] R. M. Grudzien, S. Pikus, M. Jaroniec, *J. Phys. Chem. B* **2006**, *110*, 2972 – 2975.

[51] J. Morell, G. Wolter, M. Fröba, *Chem. Mater*. **2005**, *17*, 804 – 808.

[52] M. Cornelius, F. Hoffmann, M. Fröba, *Chem. Mater*. **2005**, *17*, 6674 – 6678.

[53] L. Zhang, H. C. L. Abbenhuis, Q. Yang, Y. Wang, P. C. M. M. Magusin, B. Mezari, R. A. van Santen, *Angew. Chem.* **2007**, *119*, 5091 – 5094; *Angew. Chem. Int. Ed*. **2007**, *46*, 5003 – 5006.

[54] W. Whitenall, L. Cademartiri, G. A. Ozin, *J. Am. Chem. Soc*. **2007**, *129*, 15644 – 15649.

[55] A. Kuschel, H. Sievers, S. Polarz, *Angew. Chem.* **2008**, *120*, 9655 – 9659; *Angew. Chem. Int. Ed*. **2008**, *47*, 9513 – 9517.

[56] A. E. Kadib, P. Hesemann, K. Molvinger, J. Brandner, C. Biolley, P. Gaveau, J. J. E. Moreau, D. Brunel, *J. Am. Chem. Soc*. **2009**, *131*, 2882 – 2892.

[57] T. P. Nguyen, P. Hesemann, P. Gaveau, J. J. E. Moreau, *J. Mater. Chem*. **2009**, *19*, 4164 – 4171.

[58] L. Gao, F. Wei, Y. Zhou, X. X. Fan, Y. Wang, J. H. Zhu, *Chem. Eur. J*. **2009**, *15*, 8310 – 8318.

[59] M. P. Kapoor, S. Inagaki, *Chem. Mater*. **2002**, *14*, 3509 – 3514.

[60] B. Lee, H. Luo, C. Y. Yuan, J. S. Lin, S. Dai, *Chem. Commun*. **2004**, 240 – 241.

[61] H. I. Lee, C. Pak, S. H. Yi, J. K. Shon, S. S. Kim, B. G. So, H. Chang, J. E. Yie, Y.-U. Kwon, J. M. Kim, *J. Mater. Chem.* **2005**, *15*, 4711 – 4717;

[62] Y. Liang, M. Hanzlik, R. Anwander, *Chem. Commun*. **2005**, 525 – 527.

[63] Y. Liang, M. Hanzlik, R. Anwander, *J. Mater. Chem.* **2005**, *15*, 3919 – 3928;
[64] F. Kleitz, D. Liu, G. M. Anilkumar, I.-S. Park, L. A. Solovyov, A. N. Shmakov, R. Ryoo, *J. Phys. Chem. B* **2003**, *107*, 14296 – 14300.
[65] F. Kleitz, L. A. Solovyov, G. M. Anilkumar, S. H. Choi, R. Ryoo, *Chem. Commun*. **2004**, 1536 – 1537.
[66] S. A. El-Safty, T. Hanaoka, *Adv. Mater*. **2003**, *15*, 1893 – 1899.
[67] S. A. El-Safty, T. Hanaoka, *Chem. Mater*. **2004**, *16*, 384 – 400.
[68] H. M. A. Hunter, A. E. Garcia-Bennett, I. J. Shannon, W. Zhou, P. A. Wright, *J. Mater. Chem*. **2002**, *12*, 20 – 23.
[69] A. E. Garcia-Bennett, S. Williamson, P. A. Wright, I. J. Shannon, *J. Mater. Chem*. **2002**, *12*, 3533 – 3540.
[70] W. Zhou, H. M. A. Hunter, P. A. Wright, Q. Ge, J. M. Thomas, *J. Phys. Chem. B* **1998**, *102*, 6933 – 6936.
[71] Y. Sakamoto, I. Díaz, O. Terasaki, D. Zhao, J. Perez-Pariente, J. M. Kim, G. D. Stucky, *J. Phys. Chem. B* **2002**, *106*, 3118 – 3123.
[72] J. R. Matos, M. Kruk, L. P. Mercuri, M. Jaroniec, L. Zhao, T. Kamiyama, O. Terasaki, T. J. Pinnavaia, Y. Liu, *J. Am. Chem. Soc*. **2003**, *125*, 821 – 829.
[73] Q. Huo, D. I. Margolese, U. Ciesla, P. Feng, T. E. Gier, P. Sieger, R. Leon, P. M. Petroff, F. Schüth, G. D. Stucky, *Nature* **1994**, *368*, 317 – 321.
[74] Y. Sakamoto, M. Kaneda, O. Terasaki, D. Y. Zhao, J. M. Kim, G. D. Stucky, H. J. Shin, R. Ryoo, *Nature* **2000**, *408*, 449 – 453.
[75] P. Sakya, J. M. Seddon, R. H. Templer, R. J. Mirkin, G. J. T. Tiddy, *Langmuir* **1997**, *13*, 3706 – 3714.
[76] Q. Huo, D. I. Margolese, G. D. Stucky, *Chem. Mater*. **1996**, *8*, 1147 – 1160.
[77] H. M. A. Hunter, P. A. Wright, *Microp. Mesop. Mater*. **2001**, *43*, 361 – 373.
[78] Y. Liang, M. Hanzlik, R. Anwander, *J. Mater. Chem*. **2006**, *16*, 1238 – 1253.
[79] Y. Liang, E. S. Erichsen, M. Hanzlik, R. Anwander, *Chem. Mater*. **2008**, *20*, 1451 – 1458.
[80] J. L. Blin, C. Otjacques, G. Herrier, B.-L. Su, *Langmuir* **2000**, *16*, 4229 – 4236.
[81] A. Sayari, M. Kruk, M. Jaroniec, I. L. Moudrakovski, *Adv. Mater*. **1998**, *10*, 1376 – 1379.
[82] J. Fan, C. Yu, L. Wang, B. Tu, D. Zhao, Y. Sakamoto, O. Terasaki, *J. Am. Chem. Soc*. **2001**, *123*, 12113 – 12114.
[83] C. Vercaemst, P. E. de Jongh, J. D. Meeldijk, B. Goderis, F. Verpoort, P. Van Der Voort, *Chem. Commun*. **2009**, 4052 – 2054.
[84] D. Zhao, J. Sun, Q. Li, G. D. Stucky, *Chem. Mater*. **2000**, *12*, 275 – 279.
[85] J. M. Kim, S. K. Kim, R. Ryoo, *Chem. Commun*. **1998**, 259 – 260.
[86] P. Schmidt-Winkel, W. W. Jr. Lukens, D. Zhao, P. Yang, B. F. Chmelka, G. D. Stucky, *J. Am. Chem. Soc.* **1999**, *121*, 254 – 255.
[87] M. J. Kim, R. Ryoo, *Chem. Mater*. **1999**, *11*, 487 – 491.
[88] S. Che, S. Kamiya, O. Terasaki, T. Tatsumi, *J. Am. Chem. Soc*. **2001**, *123*, 12089 – 12090.
[89] S. H. Tolbert, C. C. Landry, G. D. Stucky, B. F. Chmelka, P. Norby, J. C. Hanson, A. Monnier, *Chem. Mater*. **2001**, *13*, 2247 – 2256.
[90] S. Brunauer, P. H. Emmett, E. Teller, *J. Am. Chem. Soc*. **1938**, *60*, 309 – 319.
[91] K. S. W. Sing, D. H. Everett, H. R. A. W. Haul, L. Moscou, R. A. Pierotti, J. Rouquérol, T. Siemieniewska, *Pure Appl. Chem*. **1985**, *57*, 603 – 619.
[92] E. P. Barrett, L. G. Joyner, P. P. Halenda, *J. Am. Chem. Soc*. **1951**, *73*, 373 – 380.